Heat Transfer—Japanese Research, 22 (2), 1993

Heat and Mass Transfer Analysis of Three-Dimensional Turbulent Flow in a Distorted Duct

Hitoshi Sugiyama and Mitsunobu Akiyama
Department of Mechanical Systems Engineering
Utsunomiya University
Masaru Hirata
Department of Mechanical Engineering
The University of Tokyo
Satoshi Ueno
Kao Co., Ltd.

A numerical analysis has been made on a three-dimensional variable area duct using a Reynolds stress equation model and including a transport-equation model for the turbulent heat flux. It is important to examine the validity of an anisotropic turbulence model for the flow in a complex configuration because we do not know the validity of the anisotropic turbulence model until we apply it. We compared the calculated results with published experimental data and made it clear that the present method was able to predict the mean flow field, but it is necessary to modify the convective and diffusion terms of the Reynolds stress equation.

Key words: Distorting duct, boundary-fitted coordinate systems, turbulent heat flux equation, algebraic stress model

1. Introduction

Research on anisotropic turbulent flows has been carried out for as long as research on isotropic ones. The latter is represented by research or grid turbulence, which was analyzed theoretically by Taylor [1] and experimentally by Dryden-Schubauer [2]. On the other hand, the study of anisotropic turbulence was reported by Townsend [3] and Tucker and Reynolds [4], who analyzed the interaction between variations in velocity distributions in the different directions and the behavior of the Reynolds stresses by experimenting on a variable are duct with continuous variation of the cross-section aspect ratio along the mean flow direction. Concerning this analysis, theoretical considerations were presented by Ribner and Tucker [5] and Batchelor-Proudman [6], who derived a predicting formula for the normal stress components. Since it only shows good predictive values for flows with abrupt velocity variations, their theory has been also called the Rapid Distortion Theory.

Simultaneously, numerous studies on anisotropic turbulence analysis have been carried out for flows through ducts of noncircular cross sections. These kinds of flows have as a peculiarity

ISSN0096–0802/93/0002–0120

the occurrence of secondary flows of the second kind, which differ from the secondary flow taking place in curved ducts due to the pressure gradient. Secondary flows of the second kind are generated by the turbulence anisotropy. Accordingly, such a secondary flow cannot be predicted by means of the conventional hypothesis of isotropic eddy viscosity. Therefore noncircular duct flows have been used as flow fields for the presentation of high-order turbulence models, of which many numerical simulation examples have been reported in recent years. The present authors, considering the secondary flow of the second kind in the flow through a rectangular duct, analyzed the differences between typical proposed turbulence models, clarifying their respective particularities [7]. Furthermore, based on the results of that analysis, we added an improvement of the specially problematic pressure-strain correlating term. The adequacy of the adopted model was verified for fully developed turbulent flow and for developing turbulent flow in a square duct [8].

On the other hand, we do not appreciate the value of any anisotropic turbulence model until we apply it to complex turbulent flows. In this study, the purpose of the present investigation was to complete an examination of an anisotropic turbulence model which was made for rather simple flows [8], adding new considerations on its adequacy, and to apply it to a flow with a complicated geometry, examining the structure of the three-dimensional turbulent flow field.

An object of the present calculation model was the distorting duct model which Tucker and Reynolds [4] employed in order to analyze the anisotropic character of turbulence. In the numerical computations, a boundary-fitted coordinate system was adopted, which simplifies the establishment of boundary conditions for the complicated geometry. The Reynolds-stress-governing equations are expressed using this boundary-fitted coordinate system.

2. Nomenclature

a : thermal conductivity

c_1, c_2, c_1^*, $c_1' c_2^*$, c_2', c_{1T}, c_{2T}, c_{1T^*}, c_{2T^*}, $c_{1T'^*}$, $c_{2T'^*}$, $c_{1T,w}$, $c_{2T,w}$, ζ, ζ^*, ζ', $c_{\epsilon T0}$, $c_{\epsilon T1}$, $c_{\epsilon T2}$, $c_{\epsilon T3}$: empirical constants

D : representative length

$f(L/x_w)$: function showing the influence of the wall

J : Jacobian

k : turbulent energy

K_1 : parameter indicating the anisotropy

P, Q, R : parameters governing the grid intervals

Re : Reynolds number = $U_{in}D/\nu$

T : time-averaged temperature

T' : fluctuating temperature

u_i : fluctuating velocity component in the i direction

$\overline{u_i u_j}$: Reynolds stress

$\overline{u_i T'}$: turbulent heat flux

U_i : time-averaged velocity component in the i direction

U_c : central mean flow velocity at $x_1 = 4$ in

U_∞ : mean flow velocity

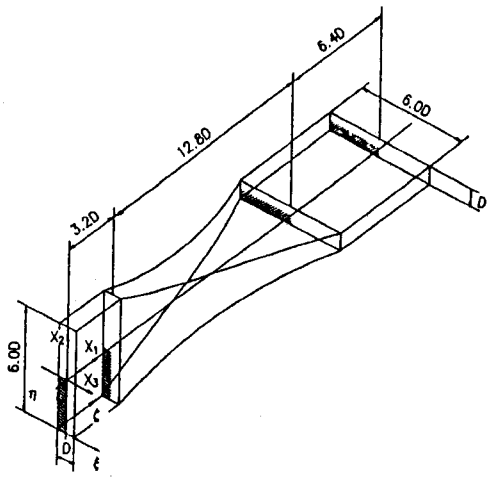

Fig. 1. Calculation region and coordinate system.

U, V, W: contravariant velocity components
U_{in}: mean flow velocity of inlet section
x_i: physical coordinate axis to the i direction
ξ, η, ζ: axes in the transformed coordinate system
ϵ: turbulent dissipation rate
ϵ_T: dissipation for the temperature fluctuation
ν: viscosity constant
π_{ij}: pressure-strain correlating term
π_{iT}: pressure-temperature gradient correlating term
ρ: density

3. Technique of Analysis

3.1 Calculation model

The model adopted for present calculations is shown in Fig. 1. The width of the rectangular cross section at the entrance is taken as the representative length D, with which all other geometrical values are expressed. Considering symmetry, calculations were performed over only one quarter of the cross section, emphasized in the figure by oblique hatching.

The distorting duct used by Tucker and Reynolds [4] whose experimental results will be compared with the present calculations consisted of three portions: First, a 2-ft-long straight entrance duct with an aspect ratio of 6:1 between the vertical and the horizontal dimensions, which included a turbulence generating grid. Second, an 8-ft-long central portion with its cross section changing progressively from an aspect ratio of 6:1 at its beginning to the final aspect ratio of 1:6 at

Table 1

Pressure–Strain Correlation

$\pi_{ij,1}+\pi_{ji,1}$	$-c_1\frac{\varepsilon}{k}\left(\overline{u_iu_j}-\frac{2}{3}k\delta_{ij}\right)$
$\pi_{ij,2}+\pi_{ji,2}$	$-\frac{c_2+8}{11}\left(P_{ij}-\frac{2}{3}P_k\delta_{ij}\right)+\zeta k\left(\frac{\partial U_i}{\partial x_j}+\frac{\partial U_j}{\partial x_i}\right)$ $-\frac{8c_2-2}{11}\left(D_{ij}-\frac{2}{3}P_k\delta_{ij}\right)$
$[\pi_{ij}+\pi_{ji}]_w$	$c_1=c_1^*+c_1'\,f\left(\frac{L}{x_w}\right),\ c_2=c_2^*+c_2'\,f\left(\frac{L}{x_w}\right),\ \zeta=\zeta^*+\zeta'\,f\left(\frac{L}{x_w}\right)$

$$P_{ij}=-\overline{u_iu_k}\frac{\partial U_j}{\partial x_k}-\overline{u_ju_k}\frac{\partial U_i}{\partial x_k}\qquad P_k=-\overline{u_ku_l}\frac{\partial U_k}{\partial x_l}$$

$$D_{ij}=-\overline{u_iu_k}\frac{\partial U_k}{\partial x_j}-\overline{u_ju_k}\frac{\partial U_k}{\partial x_i}$$

Table 2

Pressure–Temperature Gradient Correlations

$\pi_{1T,1}$	$-c_{1T}\frac{\varepsilon}{k}\overline{u_iT}-c_{1T}'\frac{\varepsilon}{k}\left(\frac{\overline{u_iu_j}}{k}-\frac{2}{3}\delta_{ij}\right)\overline{u_jT}$
$\pi_{1T,2}$	$c_{2T}\overline{u_jT}\frac{\partial U_i}{\partial x_j}-c_{2T}'\overline{u_jT}\frac{\partial U_j}{\partial x_i}$
$\pi_{iT,w}$	$c_{1T}=c_{1T}^*\{1+c_{1T,w}\,f\left(\frac{L}{x_w}\right)\}\qquad c_{1T}'=c_{1T}'^*\{1+c_{1T,w}\,f\left(\frac{L}{x_w}\right)\}$ $c_{2T}=c_{2T}^*\{1+c_{2T,w}\,f\left(\frac{L}{x_w}\right)\}\qquad c_{2T}'=c_{2T}'^*\{1+c_{2T,w}\,f\left(\frac{L}{x_w}\right)\}$

its exit. As illustrated in Fig. 1, x_1 is the mean flow direction and x_2 and x_3 are the lateral directions; the changing cross sections along the mean flow direction are given by the relation

$$x_2=(x_2)_i e^{-cx1},\quad x_3=(x_3)_i e^{cx1} \tag{1}$$

$(x_2)_i$, $(x_3)_i$ are respectively the x_2, x_3 coordinates of each wall at the entrance section, and the constant c has the value 0.22251 ft. The third portion is a 4-ft-long straight duct with an aspect ratio of 1:6, opposite from that of the entrance.

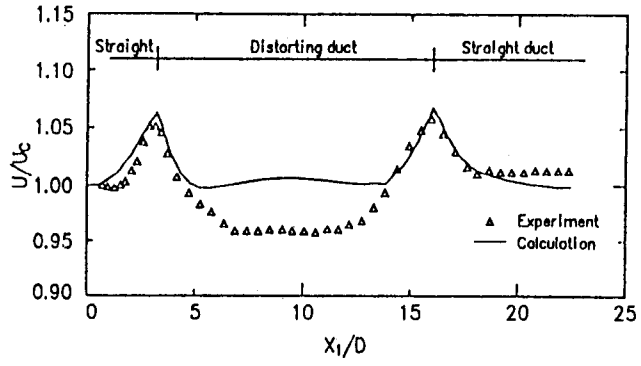

Fig. 2. The developing central velocity of the mean stream.

Flow in such an experimental device has the following behavior: As the steady flow entering the duct passes the grid, isotropic turbulence is generated. Entering the distorting duct, the turbulence turns anisotropic turbulence because of the velocity changes in the lateral direction. This change in the turbulence structure can be interpreted as the result of the redistribution of turbulent energy in each direction through the strain-pressure correlating term in the Reynolds stress equation. Entering the exit section, since the lateral velocities no longer change, the anisotropic turbulence changes to isotropic turbulence, because of the energy redistribution between the different components.

For the experimental conditions, an entrance velocity of 20 ft/s, Reynolds number (with the width of the entrance cross section as the characteristic length) $Re = 7.4 \times 10^4$ were reported. The characteristic point of the experimental conditions is the consideration of displacement thickness. This means, in order to attain a steady central velocity in the mean flow direction x_1 from the entrance to the exit, a displacement thickness is calculated at each cross section added to the cross section. This thickness is obtained from the following relation presented by Tucker [9]:

$$\delta^*(x_1) = 0.0462 x_1 \left(\frac{U_\infty x_1}{\nu}\right)^{-1/5} \tag{2}$$

The above equation gives the displacement thickness for a flat plate without pressure gradient: x_1 is the distance from the entrance and U_∞ is the mean stream velocity. In the present analysis, it was decided also to consider and calculate this thickness.

3.2 Boundary-fitted coordinate system

The calculation technique using a boundary-fitted coordinate system consists in a coordinate transformation from the analysis domain on the physical level to the calculation domain and then solving the governing equations on the calculation level. Although the specification of boundary conditions and the discretization of the equations are easy, the transformed governing

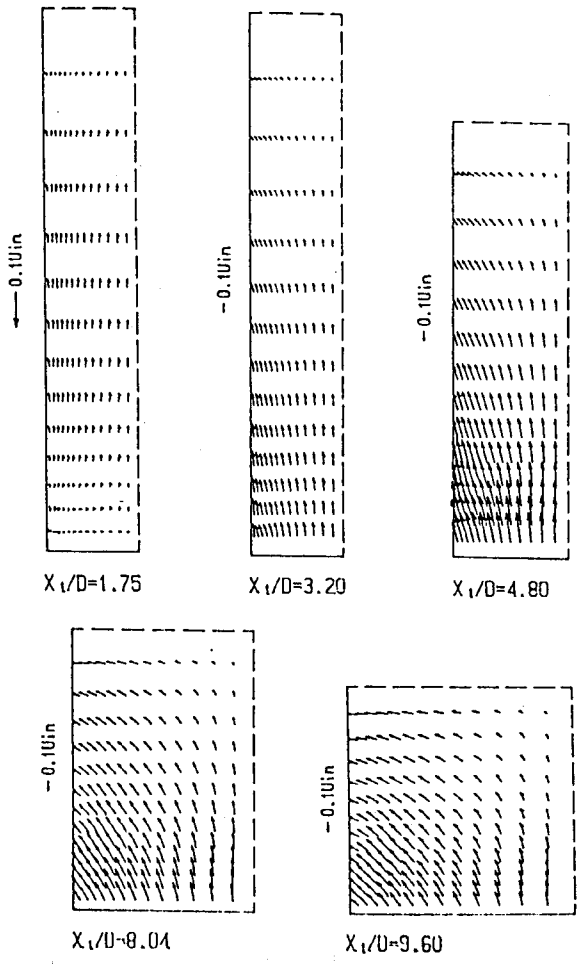

Fig. 3. The development of secondary flow.

equations are characteristically complicated. Before the calculations were carried out, the calculation mesh was previously straightened in order to achieve calculation stability and enhance convergence. In the present analysis, it was decided to solve the following kind of Poisson equation (for example, Mastin-Thompson [10]):

$$\alpha_{11}x_{\xi\xi} + 2\alpha_{12}x_{\xi\eta} + 2\alpha_{13}x_{\xi\xi} + \alpha_{22}x_{\eta\eta} + 2\alpha_{23}x_{\eta\xi} + \alpha_{33}x_{\zeta\zeta} + J^2[Px_{\xi} + Qx_{\eta} + Rx_{\zeta}] = 0$$

$$\alpha_{11}y_{\xi\xi} + 2\alpha_{12}y_{\xi\eta} + 2\alpha_{13}x_{\xi\zeta} + \alpha_{22}y_{\eta\eta} + 2\alpha_{23}x_{\eta\zeta} + \alpha_{33}y_{\zeta\zeta} + J^2[Py_{\xi} + Qy_{\eta} + Ry_{\zeta}] = 0 \quad (3)$$

$$\alpha_{11}z_{\xi\xi} + 2\alpha_{12}z_{\xi\eta} + 2\alpha_{13}z_{\xi\zeta} + \alpha_{22}z_{\eta\eta} + 2\alpha_{23}z_{\eta\zeta} + \alpha_{33}z_{\zeta\zeta} + J^2[Pz_{\xi} + Qz_{\eta} + Rz_{\zeta}] = 0$$

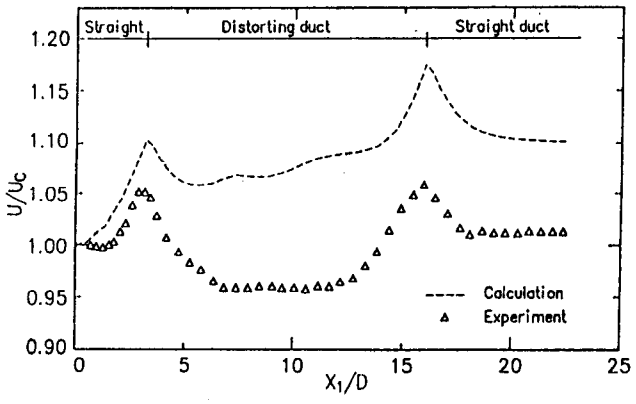

Fig. 4. The developing central velocity of the mean stream without displacement thickness.

where

$$\alpha_{jk} = \sum_{m=1}^{n=3} \beta_{mj}\beta_{mk} \tag{4}$$

$$M = \begin{bmatrix} x_\xi & x_\eta & x_\zeta \\ y_\xi & y_\eta & y_\zeta \\ z_\xi & z_\eta & z_\zeta \end{bmatrix} \tag{5}$$

ξ, η, and ζ in the above formulae are the transformed coordinate axes, on the calculation level; P, Q, and R are parameters controlling the spacing between mesh points; β_{jk} is defined as the j, k co-factor in the matrix M. Each of the subscripts, ξ, η, and ζ, indicates partial differentiation in the corresponding direction.

The transformation of the governing equations to the calculation level is accomplished according to the following mathematical definitions:

$$\frac{\partial}{\partial x_i} = \frac{\partial \xi}{\partial x_i}\frac{\partial}{\partial \xi} + \frac{\partial \eta}{\partial x_i}\frac{\partial}{\partial \eta} + \frac{\partial \zeta}{\partial x_i}\frac{\partial}{\partial \zeta} \tag{6}$$

For example, the momentum equation is transformed as follows. The equation is shown in the form of the Reynolds stress.

$$\frac{\partial U_i}{\partial t} + \frac{\partial U_i U_j}{\partial x_j} = -\frac{1}{\rho}\frac{\partial P}{\partial x_i} + \frac{\partial}{\partial x_j}\left(\nu\frac{\partial U_i}{\partial x_j} - \overline{u_i u_j}\right) \tag{7}$$

The Reynolds stress which appears in the equation is divided into a term containing the velocity gradient and a term containing the remaining.

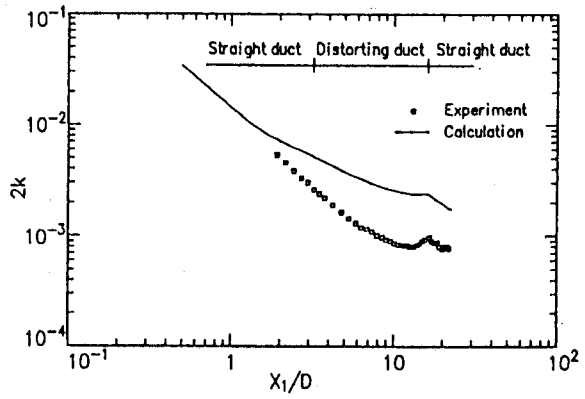

Fig. 5. The decay of turbulent energy in the mean flow direction.

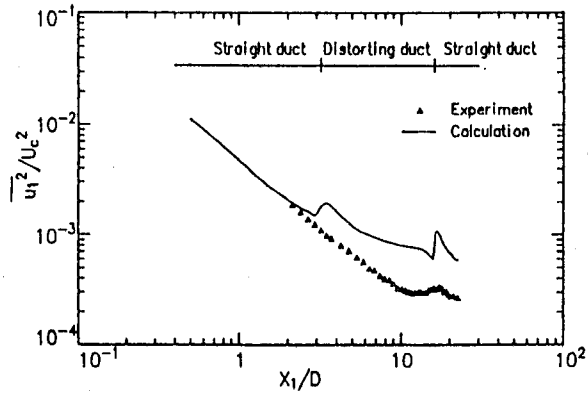

Fig. 6. The decay of normal stress $\overline{u_1^2}$ in the mean flow direction.

$$-\overline{u_i u_j} = \left(\frac{b}{a}\right)_{ij} \frac{\partial U_i}{\partial x_j} - \left(\frac{c}{a}\right)_{ij} \tag{8}$$

Here, including the Reynolds stress as part of the diffusion term in order to attain stability of the solution, we can put

$$d_{ij} = \nu + \left(\frac{b}{a}\right)_{ij} \qquad e_{ij} = \left(\frac{c}{a}\right)_{ij} \tag{9}$$

so that the momentum equation can be rewritten in the following form:

$$\frac{\partial U_i}{\partial t} + \frac{\partial U_i U_j}{\partial x_j} = -\frac{1}{\rho}\frac{\partial P}{\partial x_i} + \frac{\partial}{\partial x_j}\left(d_{ij}\frac{\partial U_i}{\partial x_j} - e_{ij}\right) \tag{10}$$

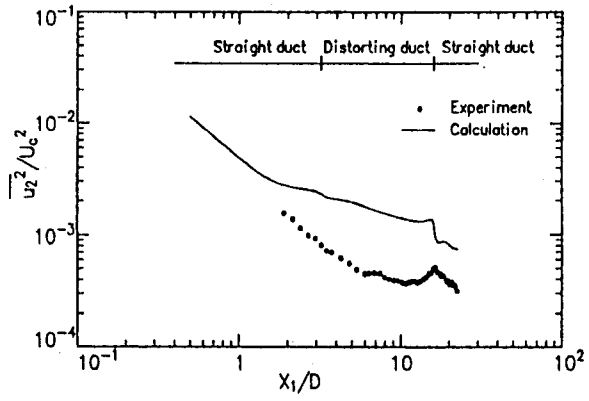

Fig. 7. The decay of the normal stress $\overline{u_2^2}$ in the mean flow direction.

Applying the mathematical definition shown above to this equation, it is finally transformed to

$$\frac{\partial U_i}{\partial t}+\frac{\partial}{\partial \xi}\left(UU_i+\frac{P}{\rho}\xi_{xi}-l_1U_{i\xi}-l_2U_{i\eta}-l_3U_{i\zeta}+\xi_{x3}e_{i3}+e_{x2}e_{i2}+\xi_{x1}e_{i1}\right)$$

$$+\frac{\partial}{\partial \eta}\left(VU_i+\frac{P}{\rho}\xi_{xi}-l_2U_{i\xi}-l_1U_{i\eta}-l_5U_{i\zeta}+\eta_{x3}e_{i3}+\eta_{x2}e_{i2}+\eta_{x1}e_{i1}\right) \tag{11}$$

$$+\frac{\partial}{\partial \zeta}\left(WU_i+\frac{P}{\rho}\xi_{xi}-l_3U_{i\xi}-l_5U_{i\eta}-l_6U_{i\zeta}+\zeta_{x3}e_{i3}+\zeta_{x2}e_{i2}+\zeta_{x1}e_{i1}\right)=0$$

$$\left.\begin{aligned}
l_1&=d_{i3}\xi_{x3}^2+d_{i2}\xi_{x2}^2+d_{i1}\xi_{xi}^2\\
l_2&=d_{i3}\xi_{x3}\eta_{x3}+d_{i2}\xi_{x2}\eta_{x2}+d_{i1}\xi_{xi}\eta_{x1}\\
l_3&=d_{i3}\xi_{x3}\zeta_{x3}+d_{x2}\xi_{x2}\zeta_{x2}+d_{i1}\xi_{x1}\zeta_{x1}\\
l_4&=d_{i3}\eta_{x3}^2+d_{i2}\eta_{x2}^2+d_{i1}\eta_{x1}^2\\
l_5&=d_{i3}\eta_{x3}\zeta_{x3}+d_{i2}\eta_{x2}\zeta_{x2}+d_{i1}\eta_{x1}\zeta_{x1}\\
l_6&=d_{i3}\zeta_{x3}^2+d_{i2}\zeta_{i2}^2+d_{i1}\zeta_{x1}^2
\end{aligned}\right\} \tag{12}$$

$$\left.\begin{aligned}
U&=U_1\frac{\partial \xi}{\partial x_1}+U_2\frac{\partial \xi}{\partial x_2}+U_3\frac{\partial \xi}{\partial x_3}\\
V&=U_1\frac{\partial \eta}{\partial x_1}+U_2\frac{\partial \eta}{\partial x_2}+U_3\frac{\partial \eta}{\partial x_3}\\
W&=U_1\frac{\partial \zeta}{\partial x_1}+U_2\frac{\partial \zeta}{\partial x_2}+U_3\frac{\partial \zeta}{\partial x_3}
\end{aligned}\right\} \tag{13}$$

where U, V, W are components of the contravariant velocity; l represents the metric tensor. In the case of a three-dimensional flow, nine diffusion coefficients are necessary. As for the other gov-

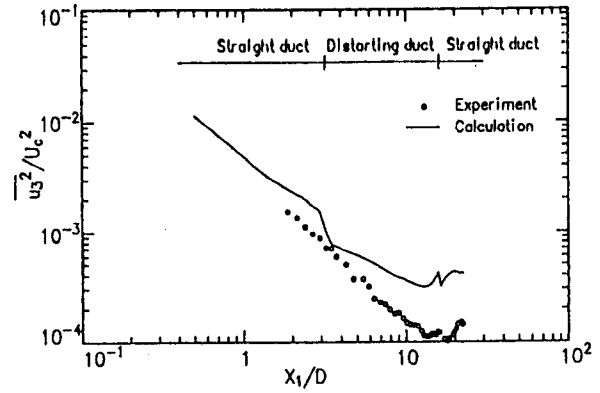

Fig. 8. The decay of normal stress $\overline{u_3^2}$ in the mean flow direction.

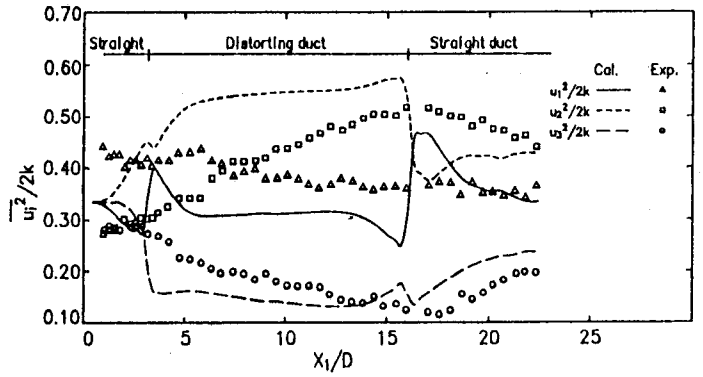

Fig. 9. The redistribution of turbulent energy among the normal stresses.

erning equations, application of the same steps leads to the transformed equations on the calculation level.

3.3 Reynolds stress equation

In order to deal correctly with the turbulence anisotropy, it was decided to solve the Reynolds stress equations. In this case, some modeling efforts are necessary. As for the particularly problematic pressure-strain correlating terms, modeling was performed according to Table 1. This model was obtained by partially improving the kinematic constraints for the fourth-order correlation tensor. It was reported in a previous work [8].

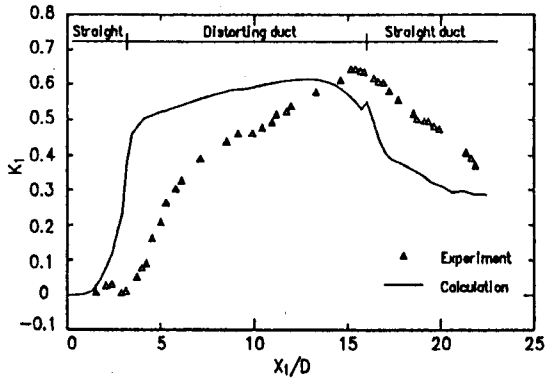

Fig. 10. The development of the anisotropic parameter K_1 in the mean flow direction.

As for the convection and the diffusion terms, their influence is taken into consideration by means of the Rodi approximation [11]. As a result of this approximation, differential equations for Reynolds stresses are transformed into algebraic equations.

3.4 Turbulent heat-flux equation

Concerning the anisotropy of temperature, it was decided to solve the turbulent heat-flux equation. Table 2 shows the modeling of the pressure-temperature correlating term, where basically the model by Lumley [12] and Launder [13] was adopted. The derivation of their model and the technique for definition of the constants are described in detail in a previous work [8]. Also as for the turbulent heat-flux equation, the previously explained Rodi's approximation [11] was applied to the temperature field, and transformed into an algebraic stress model. Actually, in extending Rodi's approximation to the temperature field, it is assumed that the production and diffusion are approximately the same.

3.5 Transport equation for temperature fluctuations and temperature dissipation

In this analysis, an attempt was made to use both the transport equation for temperature fluctuations and that for temperature dissipation. As examples of analyses involving temperature fluctuations and temperature dissipation, application to a simple shear flow field by Maekawa [14] and that to the temperature mixing layer of grid turbulence by Elghobashi-Launder [15] can be mentioned, but there are comparatively few studies of this kind. Moreover, examples of application of these transport equations to three-dimensional flow fields seem to be rare.

The strict forms of the transport equations for temperature fluctuations and temperature dissipation are as follows.

$$\frac{\partial \overline{T'^2}}{\partial t} + \frac{\partial}{\partial x_k}\left(\overline{U_k T'^2}\right) = -2\overline{u_k T'}\frac{\partial T}{\partial x_k} - 2a\overline{\frac{\partial T'}{\partial x_k}\frac{\partial T'}{\partial x_k}} \tag{14}$$

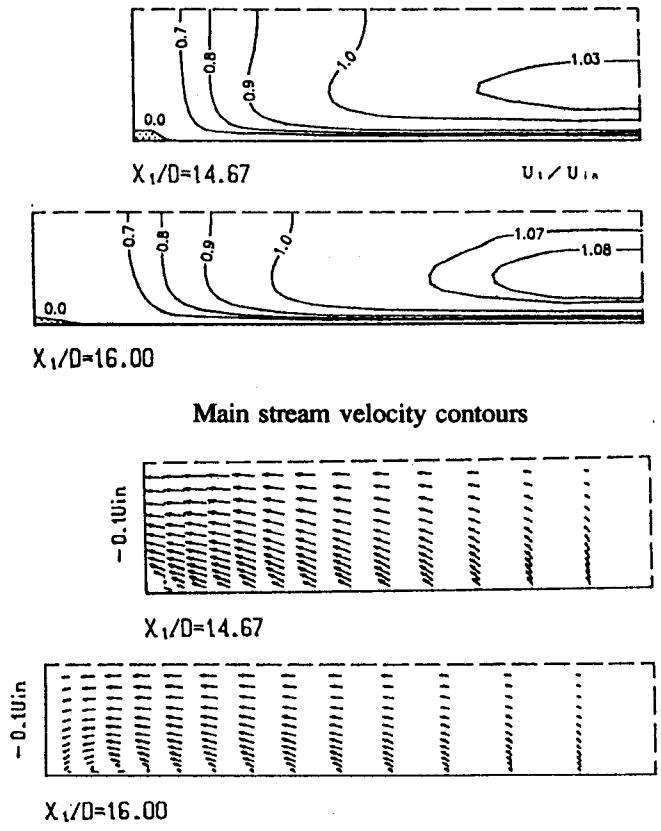

Fig. 11. Main stream velocity contours and velocity vectors of secondary flow in the separated flow region .

$$+\frac{\partial}{\partial x_k}\left(a\frac{\partial\overline{T'^2}}{\partial x_k}-\overline{u_k T'^2}\right)$$

$$\frac{\partial\varepsilon_T}{\partial t}+U_k\frac{\partial\varepsilon_T}{\partial x_k}=-2a\overline{\frac{\partial T'}{\partial x_l}\frac{\partial u_k}{\partial x_l}}\frac{\partial T}{\partial x_k}-2a\overline{u_k\frac{\partial T'}{\partial x_l}\frac{\partial^2 T}{\partial x_l\partial x_k}}$$

$$-2a\overline{\frac{\partial T'}{\partial x_l}\frac{\partial T'}{\partial x_k}}\frac{\partial U_k}{\partial x_l}-2a\overline{\frac{\partial T'}{\partial x_l}\frac{\partial u_k}{\partial x_l}\frac{\partial T'}{\partial x_k}}-2\overline{\left(a\frac{\partial^2 T'}{\partial x_l\partial x_k}\right)^2}-\frac{\partial}{\partial x_k}\left(\overline{u_k a\frac{\partial T'}{\partial x_l}\frac{\partial T'}{\partial x_l}}-a\frac{\partial\varepsilon_T}{\partial x_k}\right) \tag{15}$$

The above equations cannot be solved in these forms; a modeling is needed, which was done according to the scheme

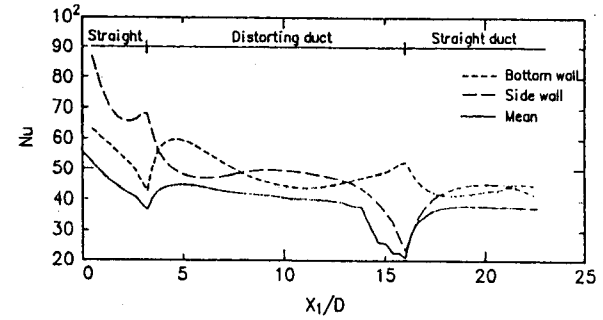

Nusselt number

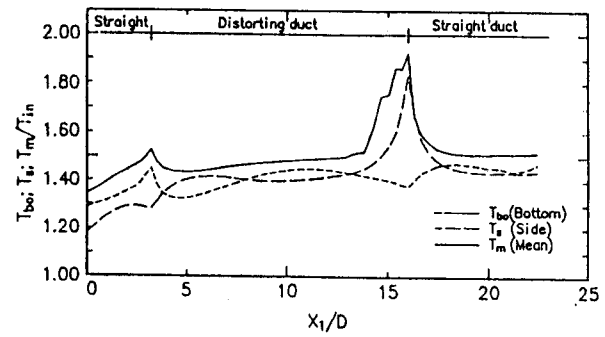

Temperature

Fig. 12. The development of temperature and Nusselt number in the flow direction.

$$\frac{\partial \overline{T'^2}}{\partial t} + \frac{\partial U_j \overline{T'^2}}{\partial x_j} = \frac{\partial}{\partial x_j}\left(c_\psi \frac{k}{\varepsilon} \overline{u_j u_l} \frac{\partial \overline{T'^2}}{\partial x_l} \right) - 2\overline{u_j T'} \frac{\partial T}{\partial x_j}$$

$$-2a\overline{\frac{\partial T'}{\partial x_j}\frac{\partial T'}{\partial x_j}} = \frac{\partial}{\partial x_j}\left(c_\psi \frac{k}{\varepsilon} \overline{u_j u_l} \frac{\partial \overline{T'^2}}{\partial x_l} \right) - 2\overline{u_j T'} \frac{\partial T}{\partial x_j} - 2\varepsilon_T \tag{16}$$

$$\frac{\partial \varepsilon_T}{\partial t} + \frac{\partial U_j \varepsilon_T}{\partial x_j} = -c_{\varepsilon T0} \frac{\overline{u_i u_j}}{k} \frac{\partial U_i}{\partial x_j} \varepsilon_T$$

$$-c_{\varepsilon T1} \frac{2\overline{u_i T'}}{\overline{T'^2}} \frac{\partial T}{\partial x_i} \varepsilon_T - c_{\varepsilon T2} \frac{\varepsilon}{k} \varepsilon_T - c_{\varepsilon T3} \frac{\varepsilon_T{}^2}{\overline{T'^2}} \tag{17}$$

where the value 0.22 was adopted for the diffusion term constant C_ψ appearing in the transport equation for fluctuating temperatures, and the values proposed by Maekawa [14] were adopted for the constants appearing in the transport equation for the fluctuating temperature dissipation.

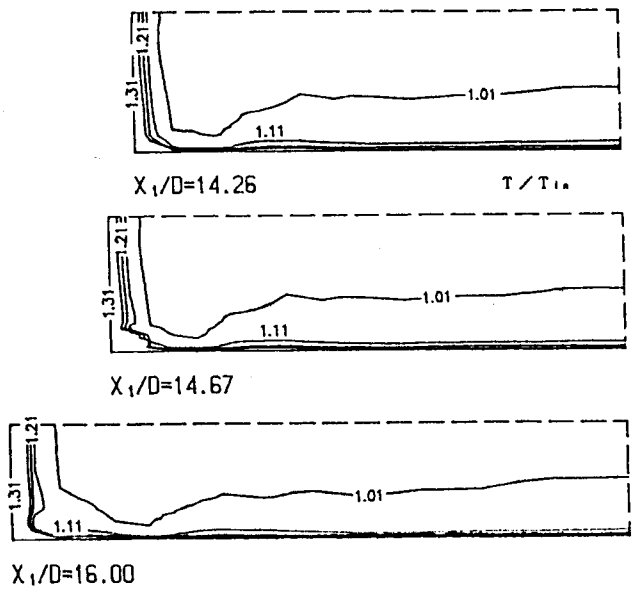

Fig. 13. The temperature isolines for a cross section near the separation region.

When solving these equations, a problem arises related to the definition of boundary conditions for temperature fluctuations and its dissipation. Here, this task is accomplished by assuming local equilibrium at the first calculation point, and a constant time-scale ratio R. With these assumptions, relations as follows are obtained as boundary conditions for the temperature fluctuation and its dissipation:

$$\overline{T'^2} = -2\frac{k}{e}\overline{u_j T'}\frac{\partial T}{\partial x_j} = -2R\frac{k}{\varepsilon}\left(\overline{u_1 T'}\frac{\partial T}{\partial x_1} + \overline{u_2 T'}\frac{\partial T}{\partial x_2} + \overline{u_3 T'}\frac{\partial T}{\partial x_3}\right) \tag{18}$$

$$\varepsilon_T = \frac{1}{R}\frac{\varepsilon}{k}\overline{T'^2} = -2\left(\overline{u_1 T'}\frac{\partial T}{\partial x_1} + \overline{u_2 T'}\frac{\partial T}{\partial x_2} + \overline{u_3 T'}\frac{\partial T}{\partial x_3}\right) \tag{19}$$

4. Results and Considerations

4.1 Analysis of the velocity field

As shown in Fig. 1, the calculation domain was taken as one-fourth of the whole cross section, in consideration of symmetry. The calculation grid was $\xi \times \eta \times \zeta = 15 \times 15 \times 50$: the Reynolds number was $Re = 7.4 \times 10^4$, having the width of the rectangular cross section at the entrance as the characteristic length. Taking the turbulence grid size as the characteristic length, the resultant Reynolds number was $Re_m = 6.8 \times 10^3$. Boundary conditions for the turbulent energy

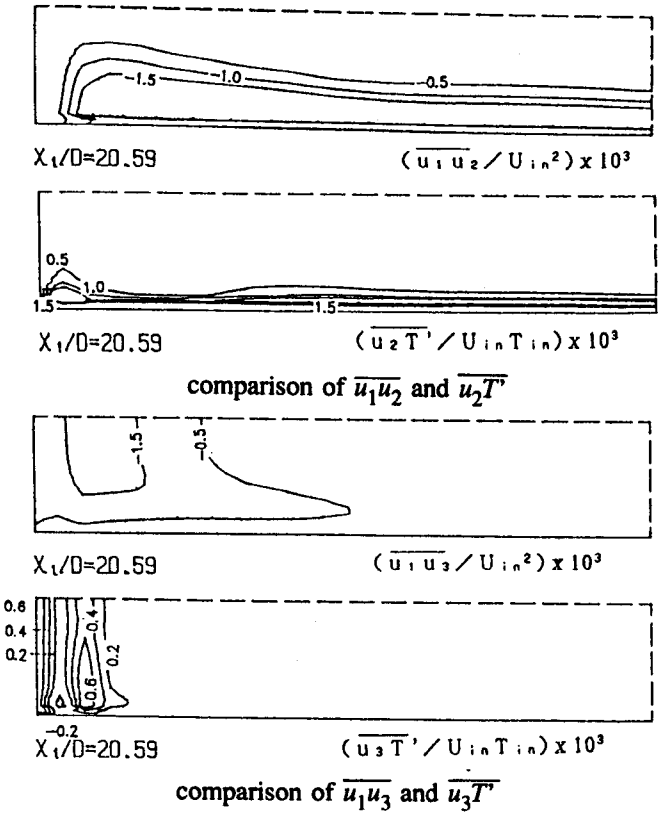

Fig. 14. The correlation between turbulent heat fluxes and Reynolds stresses.

and turbulent dissipation equations were determined at the first calculation points by means of the wall function, based on the logarithmic law of the wall and the assumption of local equilibrium. Accordingly, the smallest mesh width in the wall vicinity was selected in order to obtain a value of 40 for the dimensionless distance which is defined by the friction velocity. As in experiments, no clear statements were made about the turbulent energy and turbulent dissipation values at the entrance. Values were obtained by drawing an inference from the experimental formula for the flow past a turbulence grid. In the discretization of the governing equations, QUICK scheme (third order upwind differencing scheme) was employed for the convection terms, and a central differencing scheme was employed for the other ones.

Figure 2 shows a comparison between experimental and computational results for the developing central velocity of the mean stream. These values are normalized by the mean flow velocity at x_1 = 4 in. A peculiar feature can be noticed at the entrance and exit of the distorting duct, namely, the acceleration of the flow, which reaches a peak central velocity 6 percent higher than in the entrance section. The same tendency is clearly presented by the calculation results. Tucker [4] explains the origination of an accelerated region at the entrance of the distorting duct as follows: the high bending rates and high static pressures at the upper and lower wall cause the streamlines

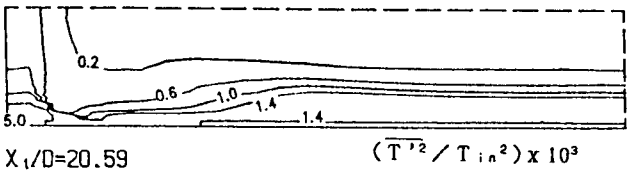

Fig. 15. The isolines for temperature fluctuation near the outlet region of the straight duct.

to turn toward the central region. However, in the calculation results, these accelerations are explained by the origination of secondary flows.

Figure 3 shows the development of secondary flow at the cross sections from x_1/D = 1.75 to 9.6. The beginning of the distorting duct corresponds to x_1/D =3.20. The figure shows that, at this position, a secondary flow with 10 percent of the velocity U_{in} at the straight duct entrance originates, going from the lower wall to the central region. As a result, the fluid quantity transported from the lower wall to the central region of the distorting duct can be the cause of the acceleration. Even at x_1/D = 1.75, which is a section at the straight entrance duct, a secondary flow with a few percent of the entrance velocity can be seen, showing that the influence of the distorting duct can be found even at an upstream position. It can be said that such a prediction can be made only when elliptical three-dimensional governing equations are used.

For ducts with noncircular cross sections, secondary flows of the second kind can occur. In the present case, however, as also suggested by its intensity, there is a predominance of secondary flow of the first kind, caused by the pressure gradients.

Figure 2 shows the calculation results when the displacement thickness is taken into account. When this thickness is neglected, calculations for the distorted duct yield the results of Fig. 4. According to this figure, the calculation results for the downstream development of the central mean stream velocity show considerable disagreement with the experimental results. This indicates that consideration of this minute displacement thickness is necessary when considering this kind of distorted duct.

The aspects of the decay of turbulent energy and of the normal stresses along the mean flow direction can be seen in Figs. 5 and 6–8, respectively, where experimental results are compared with computational results. Although there is disagreement among the absolute values, there is resemblance of the tendencies shown at the vicinity of the distorting duct exit. Actually, the larger change suffered by the calculation results at the entrance and exit of the distorting duct can be attributed to the adoption of an algebraic stress model, by means of Rodi's approximation [11] when modeling the convection and diffusion terms of the Reynolds stress equation. By using an algebraic stress model, Reynolds stresses are constituted of a characteristic quantity of the turbulence and of the velocity gradients in the different directions; among these, the values of the velocity gradients, which are directly reflected, can be the cause of the disagreement. Rodi's approximation

[11] was established assuming the change of $\overline{u_i u_j}/k$ to be slower in flow direction. Nevertheless, as in the present analysis, since a sudden change occurs at the entrance and exit sections of the distorting duct, the convection and diffusion terms require a precise consideration.

As for the behavior of the normal stress $\overline{u_3^2}$ at the distorting duct exit, the experimental results show a gradual decrease along the mean flow, followed by an increase, a peak value, a new decrease until a minimum, and finally an increase again. The same characteristic tendency can be seen in the calculations, which show the comparative adequacy of the modeling of the pressure-strain correlating term.

Figure 9 displays the distribution of turbulent energy among the normal stresses and compares them with experimental results. After flowing into the distorting duct through the pressure-strain correlating term, normal stress $\overline{u_2^2}$ increases, while the normal stress $\overline{u_3^2}$ decreases, the normal stress $\overline{u_1^2}$ remains constant. Afterward, flowing into the rectangular straight duct at the exit, the former anisotropic turbulence shows a tendency to change to an isotropic turbulence. The calculations also present a similar result. These large variations at the inlet and outlet sections can be attributed to the problem which, as mentioned before, occurs in the modeling of the diffusion and convection terms.

Townsend [3] introduced, in order to express the anisotropy of the flow, the anisotropic parameter $K_1 = \left(\overline{u_2^2} - \overline{u_3^2}\right) \Big/ \left(\overline{u_2^2} + \overline{u_3^2}\right)$, and reported, for a distorting duct with a vertical-horizontal aspect ratio 4:1, that the parameter K_1 approaches the value 0.42 independent of aspect ratio. Tucker and Reynolds obtained the value 0.64 in their experiment, disagreeing with the experimental data of Townsend. The calculation results shown in Fig. 10 are closer to the values found by Tucker and Reynolds.

A peculiar phenomenon was observed which is flow separation. Figure 11 shows the isolines of the mean stream velocity at the section at which separation occurs, and a vector plot of the secondary flow. According to the isolines, a minute region of opposing flow can be seen at the corner, for x_1/D = 14.67 to 16.00. This gives rise to the formation of a circulating pattern which can be observed in the vectors diagram, as a complicated three-dimensional flow. There are few examples of three-dimensional flow fields with separation. Nakayama, Chow, and Sharma [16] analyzed the flow in a diffuser. It is interesting that their study presents a similar phenomenon to that encountered in present calculation results. As mentioned above, the present case includes a displacement thickness at each cross section. Therefore a kind of diffuser is formed and the separation is generated.

4.2 Analysis of the temperature field

A model for the turbulent heat flux was used in the temperature field analysis. A condition of constant heat flux was assumed at the walls. As for grid number and Reynolds number, the same conditions as for the calculations of the velocity fields were used. Although different from the shape of present research, the work by Yoshida, Furuya, and Echigo [17] can be mentioned as an example of analysis on the particularities of heat transfer in a distorting duct.

Figure 12 shows the development of temperature and Nusselt number along the axes at the bottom wall center and at the side wall center, and a mean value for the walls. Nusselt numbers were calculated using the bulk temperature as a representative value. Both temperature and Nusselt numbers show significant changes at the entrance and exit regions of the distorting duct. As shown in Fig. 3, a secondary flow originates at these regions, due to the pronounced pressure gradients. Because of this convection effect, the temperature distribution and consequently the Nusselt numbers have large variations.

On the other hand, the more or less fluctuating values of Nusselt number and average wall temperature at the distorting duct exit can be attributed to the influence of the separating flow explained above. Figure 13 shows the temperature isolines for the cross sections at x_1/D = 14.26 to x_1/D = 16.00. This conjecture is supported by the constriction of the temperature isolines at the corner region at x_1/D = 14.67, which is the cross section where separating flow originates.

Next, in order to consider the correlation between heat transport and momentum transport, a comparison is made between the values of Reynolds stresses and the turbulent heat flux at the exit straight duct, at x_1/D = 20.59. Figure 14 shows isolines for shear stress $\overline{u_1u_2}$ and turbulent heat flux $\overline{u_2T'}$, and $\overline{u_1u_3}$ and $\overline{u_3T'}$. Shear stress $\overline{u_1u_2}$ and turbulent heat flux $\overline{u_2T'}$ show a development in the x_2 direction, while $\overline{u_1u_3}$ and $\overline{u_3T'}$ show a development in the x_3 direction. This common feature in the distributions is observed, but it can hardly be said that a similarity between heat transfer and momentum transfer exists.

Since there are few examples of solutions of temperature fluctuations and temperature dissipation in three-dimensional turbulent flow fields, in the present analysis an attempt was made to solve the transport equations for those quantities. Figure 15 shows the isolines for temperature fluctuation at x_1/D = 20.59, in the exit of the straight duct. At this position, higher values exist at the bottom wall than at the lateral wall, and the high values at the corner region can be mentioned as a particular phenomenon.

5. Conclusion

The real worth of an anisotropic turbulence model is only manifested when it is applied to a complicated flow by which it is required as a special treatment. In this study, the Reynolds stress equation and turbulent heat flux equation were modeled and a boundary-fitted coordinate system was introduced, facilitating the definition of boundary conditions, and an attempt was made to analyze a three-dimensional turbulent heat transfer, leading to the following conclusions.

(1) For the prediction of the average flow field, comparatively good results were obtained. The same cannot be said with respect to the decay in normal stresses, where disagreement with experimental results were seen. However, the decay pattern is somewhat similar.

(2) For cases with intensive changes in the flow, in addition to Rodi's approximation, further modeling is needed for the diffusion and convection term.

(3) In order to solve the flow field treated in present research, consideration of the displacement thickness in the calculations is necessary.

(4) In the flow field treated in this analysis, the separating flow over a small region can be mentioned as a peculiar phenomenon.

(5) Through this model, it was possible to express the energy redistribution between the normal stresses, which showed the adequacy of the modeling of the pressure-strain correlating terms.

(6) Transport equations for temperature fluctuations and for its dissipation were introduced. A technique of analysis of a three-dimensional anisotropic turbulent temperature field including a model for the turbulent heat flux was presented.

We express our gratitude to the Ministry of Education of Japan for the assistance through its Scientific Research Fund (Research Encouragement A).

Literature Cited

1. G.I. Taylor. 1935. *Proc. London*, Ser. A. 151, 421–478.
2. H.L. Dryden, G.B. Schubauer, G.B. Mock, and H.K. Skarmstad. 1973. NASA Rep., No. 581.
3. A.A. Townsend. 1945. *Q. J. Mech. Appl. Math.*, **7**, 104–127.
4. H.J. Tucker and A.J. Reynolds. 1968. *J. Fluid Mech.*, **32**, 657–673.
5. H.S. Ribner and M. Tucker. 1952. MACA Tech. Note, 2606.
6. G.K. Batchelor and I. Proudman. 1954. *Q. J. Mech. Appl. Math.*, **7**, 83–103.
7. M. Akiyama, H. Kawamura, T. Serizawa, H. Sugiyama, T. Kunugi, and I. Nishiwaki. 1989. *Trans. JSME*, **55** (510), B, 351–357.
8. H. Sugiyama, M. Akiyama, and T. Serizawa. 1990. *Trans. JSME*, **56** (531), B, 3328–3335.
9. H.J. Tucker. 1966. Tech. Note, *McGill Univ. Mech. Eng. Res. Labs.*, **66** (4).
10. C.W. Mastin and J.F. Thompson. 1978. *Number, Math.*, **29**, 397–407.
11. W. Rodi. 1976. *Z. Angew. math. Mech.*, **56**, 219–221.
12. J.L. Lumley. 1975. Lecture Ser., von Karman Inst. Belgium, No. 76.
13. B.E. Launder. 1979. *Turbulent Shear Flows*, I. Springer-Verlag, 259–278.
14. H. Maekawa, M. Kobayashi, K. Kazama, and T. Satoh. 1979. *Trans. JSME*, **45** (395), B, 694–704.
15. S. Elghobashi and B.E. Launder. 1981. *Proc., 3rd Symp. Turbulent Shear Flows*, 15.13–15.17, Davis.
16. A. Nakayama, W. Chow, and D. Sharma. 1983. *Trans. JSME*, **49** (447), B, 2483–2486.
17. H. Yoshida, T. Furuya, and R. Echigo. 1989. *Turbulent Shear Flows*, **6**. Springer-Verlag, 269.

□♦♦♦□

Originally published in *Trans. JSME*, B, **57** (539), 1991, 2269–2276.
Translated by Hitoshi Sugiyama, Department of Mechanical Systems Engineering, Utsunomiya University, 2753 Ishii-cho Utsunomiya 321, Japan.